Fingerprints of Galactic Loop I on the Cosmic Microwave Background

Liu, Hao; Mertsch, Philipp; Sarkar, Subir

Published in:
The Astrophysical Journal Letters

DOI:
10.1088/2041-8205/789/2/L29

Publication date:
2014

Document version
Early version, also known as pre-print

The Astrophysical Journal Letters, 789:L29 (5pp), 2014 July 10 doi:10.1088/2041-8205/789/2/L29

FINGERPRINTS OF GALACTIC LOOP I ON THE COSMIC MICROWAVE BACKGROUND

Hao Liu[1,2], Philipp Mertsch[3], and Subir Sarkar[4,5]
[1] Niels Bohr Institute and Discovery Center, Copenhagen University, Blegdamsvej 17, DK-2100 Copenhagen Ø, Denmark; liuhao@nbi.dk
[2] Institute of High Energy Physics, CAS, Beijing, China
[3] Kavli Institute for Particle Astrophysics and Cosmology, 2575 Sand Hill Road, M/S 29, Menlo Park, CA 94025, USA
[4] Rudolf Peierls Centre for Theoretical Physics, University of Oxford, 1 Keble Road, Oxford OX1 3NP, UK
[5] Niels Bohr International Academy, Copenhagen University, Blegdamsvej 17, DK-2100 Copenhagen Ø, Denmark
Received 2014 April 7; accepted 2014 June 11; published 2014 June 20

ABSTRACT

We investigate possible imprints of galactic foreground structures such as the "radio loops" in the derived maps of the cosmic microwave background. Surprisingly, there is evidence for these not only at radio frequencies through their synchrotron radiation, but also at microwave frequencies where emission by dust dominates. This suggests the mechanism is magnetic dipole radiation from dust grains enriched by metallic iron or ferrimagnetic molecules. This new foreground we have identified is present at high galactic latitudes, and potentially dominates over the expected *B*-mode polarization signal due to primordial gravitational waves from inflation.

Key words: cosmic background radiation – cosmology: observations – polarization

Online-only material: color figures

1. INTRODUCTION

The study of the cosmic microwave background (CMB) radiation is a key testing ground for cosmology and fundamental physics, wherein theoretical predictions can be confronted with observations (Larson et al. 2011; Ade et al. 2013a, 2013b). The temperature fluctuations in the CMB have provided our deepest probe of the big bang model and of the nature of spacetime itself. Moreover, CMB data provide a bridge between cosmology and astro-particle physics, shedding light on galactic cosmic rays (Mertsch & Sarkar 2013), and galactic X- and γ-ray emission (Aghanim et al. 2011, 2012; Ade et al. 2013d).

Since the first release of data from the *Wilkinson Microwave Anisotropy Probe* (*WMAP*), it has been noted that the derived CMB sky maps exhibit departures from statistical isotropy (Chiang et al. 2003, 2008; de Oliveira-Costa et al. 2004; Copi et al. 2004, 2007; Schwarz et al. 2004; Park 2004; Eriksen et al. 2004; Land & Magueijo 2005, 2007; Cruz et al. 2008; Hoftuft et al. 2009; Hansen et al. 2009; Kim & Naselsky 2010; Gruppuso et al. 2013), probably because of residuals from the incomplete removal of galactic foreground emission. For example, the Kuiper Belt in the outer solar system may partly be responsible for the unexpected quadrupole–octupole alignment and parity asymmetry in the CMB (Hansen et al. 2012). This issue has acquired even more importance after the first release of cosmological data products from the *Planck* satellite (Ade et al. 2013c).

In this Letter, we construct a physical model to account for the local features of the *WMAP* internal linear combination (ILC) map (Bennett et al. 2013) in the direction of the galactic "radio loops," in particular Loop I (Berkhuijsen et al. 1971). We show that in the low multipole domain, $\ell \leqslant 20$, the peaks of the CMB map *correlate* with radio synchrotron emission from Loop I. However, the physical source of this anomaly is likely related to emission by dust—including magnetic dipole emission from dust grains enriched by metallic Fe, or ferrimagnetic materials like Fe_3O_4 (Draine & Lazarian 1999; Draine & Hensley 2013).

The radio loops are probably old supernova remnants (SNRs) in the radiative stage which have swept up interstellar gas, dust, and magnetic field into a shell-like structure. Dust grains are well-coupled to the gas by direct collisions, Coulomb drag, and Lorentz forces. Hence along with synchrotron radiation by high energy electrons, dust emission will be enhanced in the shell, with limb-brightening yielding the observed ring-like morphology. Moreover, part of the Loop I anomaly overlaps with the *Planck* haze at 30 GHz (Ade et al. 2013d). We are investigating these issues in more detail and will present the results elsewhere.

The structure of this Letter is as follows. In Section 2, we summarize the properties of Loops I–IV from radio waves to γ-rays. In Section 3, we demonstrate that there are spatial correlations between features in the *WMAP* 9 yr ILC map of the CMB and Loop I—the CMB temperature is systematically shifted by $\sim$20 μK along Loop I. We perform a cluster analysis along the Loop I radio ring and show that the peaks in the CMB map are indeed clustered in this ring with a chance probability of $\sim 10^{-4}$. In Section 4, we discuss how this signal from Loop I could have evaded foreground subtraction using the ILC method. In Section 5, we discuss physical mechanisms of the emission from the Loop I region and argue that it likely arises from interstellar dust, possibly including magnetic dipole radiation from magnetic grain materials. We present our conclusions in Section 6.

2. THE RADIO LOOPS IN THE MILKY WAY

Radio surveys of the Galaxy reveal a number of features that are parts of larger "radio loops" (Berkhuijsen et al. 1971). The most prominent is the North-Polar Spur (NPS) which is part of Loop I (Roger et al. 1999). It has been noted that the radio loops correlate with expanding shells of gas and dust, energized by supernovae (SNe) or stellar winds (Berkhuijsen et al. 1971; Heiles et al. 1980; Salter 1983; Wolleben 2007). The Loop I superbubble has been attributed to stellar winds from the Sco-Cen OB association and SN activity, with the NPS being the brightest segment of a SNR. The ambient magnetic field is most likely draped around the expanding bubbles (Heiles et al. 1980), as seen in radio and optical polarization data. The NPS

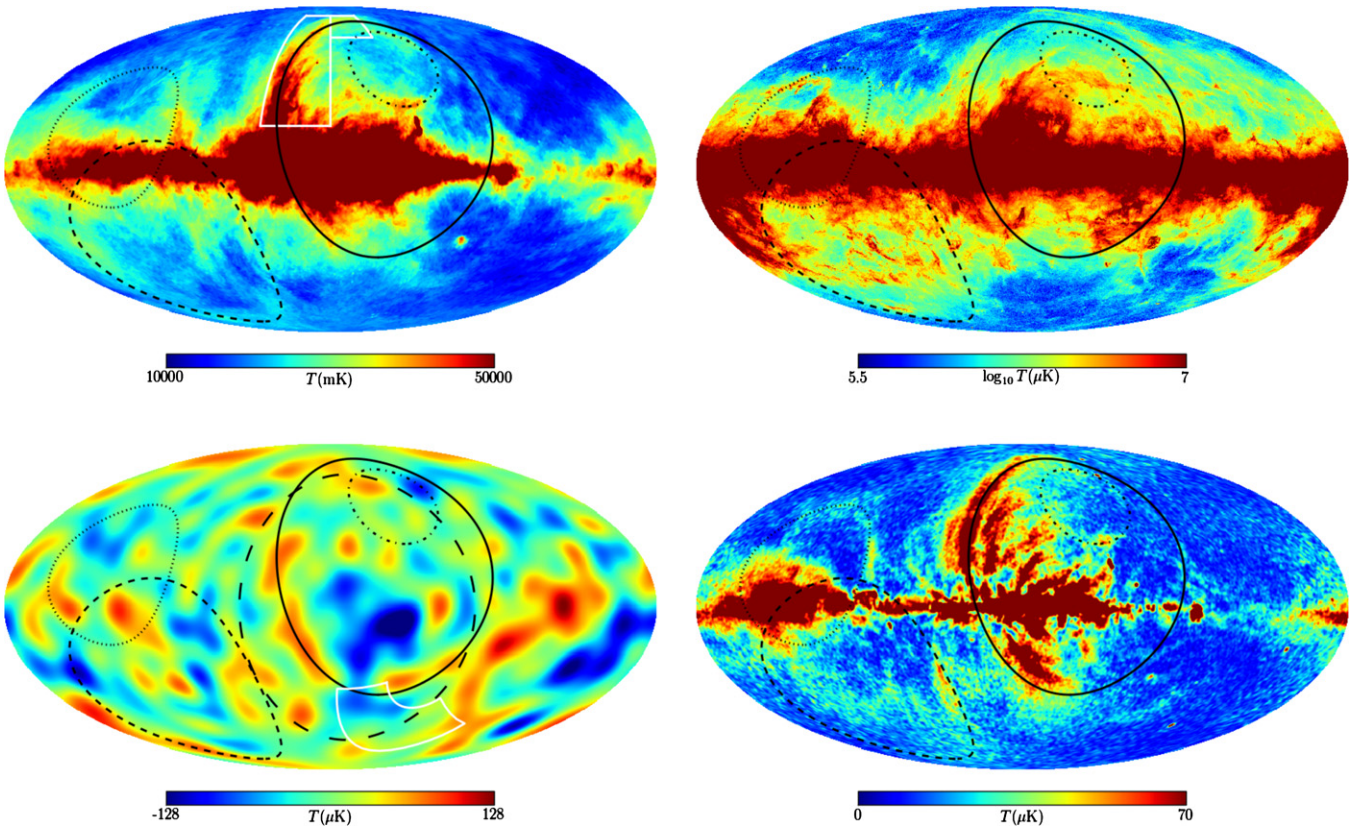

Figure 1. 408 MHz survey (top left), the *Planck* 857 GHz map (top right), the low resolution ($l \leqslant 20$) *WMAP*9 ILC map (bottom left), and the *WMAP*9 *K*-band polarized intensity map (bottom right), with the positions of the radio loops indicated: Loops I–IV are indicated by the solid, dashed, dotted, and dash-dotted lines, respectively, and "Wolleben's loop S1" by the long-dashed line. The white outline (top left panel) marks the NPS at 22 MHz, and the BICEP2 observation region is also indicated (bottom left panel).

(A color version of this figure is available in the online journal.)

is observed over a wide range of wavelengths—the 408 MHz and 1.4 GHz all-sky surveys, the *ROSAT* X-ray surveys at 0.25, 0.75, and 1.5 keV, and soft and hard γ-ray sky maps from EGRET and *Fermi*-LAT. It has also been detected in the *WMAP* *K*-band intensity and polarization maps, and more recently in the 2013 *Planck* 30 GHz temperature map (Ade et al. 2013a), and even in the 353–857 GHz far-IR maps. Hansen et al. (2012) have suggested from a cross-correlation of Faraday rotation and *WMAP* maps that such structures may affect the measured CMB temperature at high galactic latitudes.

We adopt the properties of Loops I–IV as given in Table 1 of Berkhuijsen et al. (1971). In Figure 1 we show the 408 MHz all-sky survey (Haslam et al. 1982), the 2013 *Planck* 857 GHz map, the *WMAP*9 *K*-band polarization intensity map, and the *WMAP*9 low resolution ($\ell \leqslant 20$) ILC map of the CMB—hereafter called "ILC9." We have superimposed the loops and the NPS, as well as the sky region observed by BICEP2 (Ade et al. 2014).

3. CMB PEAKS ALONG LOOP I

To investigate possible correlations between the radio loops and features in the ILC9 map, we examine a ring of width $\pm 2^\circ$ along Loop I. The average temperature of the ILC9 signal along the $\pm 2^\circ$ ring, $\overline{T} = (2\pi)^{-1} \int_0^{2\pi} d\Phi\, (T_{\rm ILC}(\Phi) - \overline{T}_{\rm ILC}) \simeq 23.9\,\mu$K, deviates significantly from the expectation for a random realization of the CMB. In order to quantify this, we have generated 1000 CMB realizations of the *WMAP* best-fit ΛCDM cosmological model (Bennett et al. 2013). Computing the number of simulated realizations with an average temperature equal or larger than the observed $\overline{T} = 23.9\,\mu$K, we find a p-value of only 0.01.

We have also determined the skewness of the distribution of ILC9 temperatures along the $\pm 2^\circ$ Loop I ring: $\gamma_1 = 1/(2\pi) \int_0^{2\pi} d\Phi[(T_{\rm ILC}(\Phi) - \overline{T}_{\rm ILC}(\Phi))/\sigma]^3 \simeq -0.68$, where σ is the standard deviation of the ILC9 temperatures. Comparing this with the skewness of 1000 Monte Carlo (MC) simulations we find a similarly small p-value of 0.03.

These anomalies warrant a more detailed analysis. In order to show the result more clearly, we have investigated the statistical isotropy in a $\pm 10^\circ$ ring around Loop I, using a cluster analysis (Naselsky & Novikov 1995) that has been applied previously to *WMAP* data (Naselsky et al. 2004): if the ILC9 map is statistically isotropic, there should be *no* correlation between the position of its peaks and the position of Loop I. We therefore test the hypothesis that the distribution of the positive peaks around Loop I is *not* random.

To quantify this, we compute for each pixel the angular distance G from Loop I along great circles crossing both the pixel and the loop center. Figure 2 shows the average distance $\langle G \rangle$ for all pixels in a $\pm 10^\circ$ wide ring around Loop I, averaged in $\Delta T = 3\,\mu$K bins. It is apparent that on average, pixels with higher temperature are closer to Loop I, i.e., the peaks in the ILC9 map *are* clustered along Loop I. To quantify the chance probability of this, we have generated 100,000 CMB maps from the *WMAP* best-fit ΛCDM cosmological model (Bennett et al. 2013). We determine the fraction of mock maps that have an average angular distance g_i smaller than the observed angular

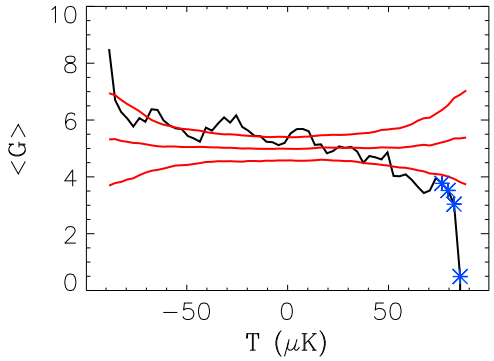

Figure 2. Average angular distance to Loop I vs. temperature. The curve is descending, indicating that higher temperature pixels are closer to Loop I. The red lines show the $\pm 1\sigma$ range, while the four highest temperature bins are marked by asterisks.

(A color version of this figure is available in the online journal.)

Table 1
The Probabilities for $g_i < G_i$ ($i = 1 \sim 4$) for the Highest Four Bins Under Different Criteria, Evaluated with 100,000 MC Simulations

Criterion	Probability (%)
$g_i < G_i$ for all four bins	0.018
$g_i < G_i$ for any three in four bins	2.0
$g_i < G_i$ for any two in four bins	3.3
$g_i < G_i, i = 1$ ($T = 84$–$87\,\mu$K)	0.1
$g_i < G_i, i = 2$ ($T = 81$–$84\,\mu$K)	2.9
$g_i < G_i, i = 3$ ($T = 78$–$81\,\mu$K)	7.5
$g_i < G_i, i = 4$ ($T = 75$–$78\,\mu$K)	8.6
$\sum_i g_i < \sum_i G_i, i = 1 \sim 4$	1.0

distance G_i in bin i. Only 18 of the 100,000 mock maps satisfy $g_i < G_i$ for all four last bins. In Table 1, we list the probabilities for the clustering around Loop I to occur by chance, adopting different criteria. In the sky map in Figure 3, the pixels in the four highest temperatures bins are marked white, while the pixels in the fifth (sixth and seventh) highest temperature bins are marked gray (black). We have checked the effect of applying the *WMAP* ILC mask on the anomalies in mean, skewness and clustering and we find our results to be largely unchanged.

4. THE LOOP I ANOMALY AS A RESIDUAL FROM THE CMB FOREGROUNDS SEPARATION

We turn now to the question of how a *physical* loop emission could have evaded the foreground cleaning process. The ILC method for isolation of the CMB signal is based on the independence of its temperature on frequency. The temperature $S_j(\hat{\mathbf{n}})$ in frequency band j and direction $\hat{\mathbf{n}}$ is a superposition of the primordial CMB $c(\hat{\mathbf{n}})$ and other components:

$$S_j(\hat{\mathbf{n}}) = c(\hat{\mathbf{n}}) + F_j(\hat{\mathbf{n}})\,, \tag{1}$$

where $F_j(\hat{\mathbf{n}}) = F_j^{\rm dust}(\hat{\mathbf{n}}) + F_j^{\rm synch}(\hat{\mathbf{n}}) + \cdots + N(\hat{\mathbf{n}})$ is the sum of dust, synchrotron and other foregrounds, as well as instrumental noise.

For regions of the sky outside the galactic mask, the estimator of the CMB anisotropy $d(\hat{\mathbf{n}})$ is given by an ILC of the N different frequency bands:

$$d(\hat{\mathbf{n}}) = \sum_j W_j S_j(\hat{\mathbf{n}}) = c(\hat{\mathbf{n}}) + \sum_j W_j F_j(\hat{\mathbf{n}})\,. \tag{2}$$

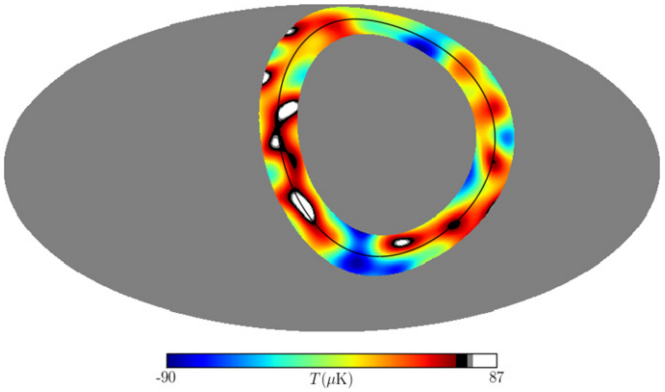

Figure 3. ILC9 temperature in a $\pm 10^\circ$ ring around Loop I. The white zones correspond to the four bins with the highest temperature, the gray zones show the effect of adding the next bin, and the black zones indicate the effect of adding two more bins.

(A color version of this figure is available in the online journal.)

The weights are chosen so as to preserve unit response to the CMB, i.e., $\sum_j W_j = 1$, and to minimize contamination by foregrounds. The reconstruction of the CMB $c(\hat{\mathbf{n}})$ through the estimator $d(\hat{\mathbf{n}})$ is exact, if and only if

$$\varepsilon(\hat{\mathbf{n}}) \equiv d(\hat{\mathbf{n}}) - c(\hat{\mathbf{n}}) = \sum_j W_j F_j(\hat{\mathbf{n}}) = 0. \tag{3}$$

Since the coefficients W_j are independent of $\hat{\mathbf{n}}$, Equation (3) presumes that the frequency dependence of the foregrounds is also *independent* of $\hat{\mathbf{n}}$. For example for a component with an assumed power-law frequency dependence like the dust emission:

$$F_j^{\rm dust}(\hat{\mathbf{n}}) = F_0^{\rm dust}(\hat{\mathbf{n}}) \left(\frac{\nu_j}{\nu_0}\right)^{\alpha_j}\,, \tag{4}$$

the α_j are taken to be constants, i.e., the morphology of the foregrounds is assumed to be the *same* in all bands. Here, ν_j is the frequency of the jth band, while $F_0^{\rm dust}(\hat{\mathbf{n}})$ is the foreground sky map at the reference frequency ν_0.

In practice this assumption cannot be fully valid since the transition from low frequencies to high frequencies leads to significant variability of the spectral index $\alpha_j(\hat{\mathbf{n}})$. Clearly, no method for optimization of the difference $d(\hat{\mathbf{n}}) - c(\hat{\mathbf{n}})$ can be free from the residuals of foreground emissions for which $\varepsilon(\hat{\mathbf{n}}) \neq 0$. There is also an ultimate limit to the accuracy with which the CMB map can be reconstructed due to its chance correlations with the foregrounds. Consequently, some areas of the reconstructed CMB map may be contaminated by foreground residuals. An example is the contamination of the ILC map by residuals after removal of point sources, which produces non-Gaussian features in the derived CMB signal. We now show that a similar effect may be causing the anomaly in the Loop I region.

We consider a simple model. Suppose that between frequencies $\nu_{\rm min}$ and $\nu_{\rm max}$ (corresponding to bands $\{j\} = \{1, \ldots, N_c\}$ of the N frequency bands) the area of Loop I is contaminated by an anomalous black body emission with temperature $T_s \sim 20\,{\rm K} \gg T_{\rm CMB}$ and optical depth $\tau \sim 10^{-6}$, modifying Equation (1) to

$$S_j(\hat{\mathbf{n}}) = c(\hat{\mathbf{n}}) + F_j(\hat{\mathbf{n}}) + \tau(\hat{\mathbf{n}}) T_s \Theta(\nu_{\rm min} \leqslant \nu_j \leqslant \nu_{\rm max})\,. \tag{5}$$

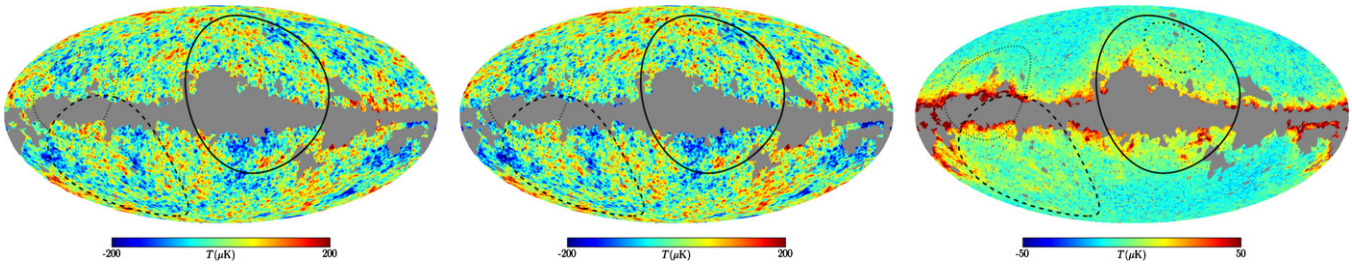

Figure 4. ILC map generated using $W_j^{\rm rest}$ (left), $W_j^{\rm LoopI}$ (middle), and their difference (right), with the radio loops superimposed.
(A color version of this figure is available in the online journal.)

The error function $\varepsilon(\hat{\mathbf{n}})$ is then

$$\varepsilon(\hat{\mathbf{n}}) = \sum_{j=1}^{N} W_j F_j(\hat{\mathbf{n}}) + \sum_{j=1}^{N_c} W_j \tau(\hat{\mathbf{n}}) T_s. \quad (6)$$

The second term, will make an anomalous contribution to the reconstructed CMB signal in the Loop I region. If this anomaly has the same frequency dependence as the other foregrounds considered, the ILC method would have efficiently suppressed its contribution. Conversely, the existence of the observed anomaly (Section 3) implies that, at least locally (in this case in the direction of Loop I), its spectrum must be *different*.

We can estimate the spectrum of the anomalous emission from the weight coefficients $W_j^{\rm LoopI}$ derived from a particularly bright part of Loop I, and those $W_j^{\rm rest}$ derived from the CMB sky (with the 9 yr KQ85 mask) *excluding* the Loop I region. We adopt a minimal variance approach (see Chiang et al. 2008; Bennett et al. 2013 for details) and find for the *WMAP K*, *Ka*, *Q*, *V*, *W* bands: $W_j^{\rm rest} = (-0.181, -0.073, 0.846, 0.460, -0.052)$ and $W_j^{\rm LoopI} = (-0.420, 0.082, 1.654, 0.309, -0.625)$. Since Loop I covers a small fraction of the sky, the weight coefficients for the sky (outside the mask) are similar whether or not the Loop I region is included.

However, the weights for the Loop I region and for the rest of the sky are *different*. In Figure 4 we show the ILC maps obtained with both sets of coefficients and their difference map which clearly indicates the presence of the loops. This means that the anomaly is efficiently suppressed by the $W_j^{\rm LoopI}$. We have checked which power-law indices β are "zeroed" by these weights, finding these to be synchrotron-like ($\beta \sim -3$), and one higher $\beta \sim 1.4$, i.e., dust-like but somewhat flatter. We caution that this is not definitive, e.g., because variation of dust temperature and temperature conversion factors are ignored.

5. PHYSICAL MODELS OF THE PEAKS ALONG LOOP I

Adopting the synchrotron model (Sarkar 1982; Mertsch & Sarkar 2013) for the radio loops, we have produced maps (with $l \leqslant 20$) for Loop I at *WMAP* frequencies (22.8–93.5 GHz). With the $W_j^{\rm rest}$ from above, the minimum variance method suppresses the contribution from Loop I to the ILC map, $T_{\rm ILC,synch} = \sum_{j=1}^{N} W_j^{\rm rest} T_{\rm synch}(\nu_j)$, to 2 μK, compared to $T_{\rm synch}(22.8\,{\rm GHz})$ of 160 μK. To get a synchrotron contribution to the ILC map of 20 μK by extrapolating from 408 MHz, the spectral index would need to be -2.4 (for $W_j^{\rm rest}$ and $W_j^{\rm loop}$, respectively) or even as hard as -2.0 (for the *WMAP* region 0 coefficients). We conclude therefore that synchrotron emission *cannot* be responsible for the anomalies in the *WMAP* ILC map, and we should look instead at emission by dust. As noted earlier, the two emissions are expected to be spatially *correlated* in the shells of old SNRs like Loop I.

To further investigate the frequency dependence we have studied the correlation of the ILC temperature map $T_{\rm ILC}$ with the *WMAPW*- and *V*-band maps of polarized intensity in temperature units, P_W and P_V. The latter have not entered into the production of the ILC map and are furthermore expected to be dominated by polarized dust. Therefore, their correlation with the ILC map gives us an *independent* handle on the contamination of the Loop I region by dust emission. We have computed the ratio of the polarized intensity in the *W*- and *V* band, averaged over the $\pm 10^\circ$ wide ring (see Figure 3) and find $\overline{P_W/P_V} = 1.7$ (which changes by less than 5% with a different ring width e.g., $\pm 2^\circ$). If the temperature anisotropy in this sample is weakly dependent on frequency ν, and $T(\nu) \approx \overline{T} \simeq 23\,\mu$K (at least for the *WMAP V* and *W* bands) this value of 1.7 indicates the existence of *two* dust components in the Loop I region by the following argument.

Suppose that the anomalous emission is associated with a single thermal dust component. According to the *Planck* all-sky dust emission model (Abergel et al. 2013a, 2013b), the temperature of the dust in units of the CMB thermodynamic temperature in the direction $\hat{\mathbf{n}}$ is

$$T(\nu, \hat{\mathbf{n}}) = T(\nu_0, \hat{\mathbf{n}}) \frac{c(\nu)}{c(\nu_0)} \frac{e^{\frac{h\nu_0}{kT_{\rm dust}(\mathbf{r})}} - 1}{e^{\frac{h\nu}{kT_{\rm dust}(\hat{\mathbf{n}})}} - 1} \left(\frac{\nu}{\nu_0}\right)^{\beta(\hat{\mathbf{n}})+1},$$
$$c(\nu) = \left(2 \sinh \frac{x}{2} \Big/ x\right)^2, \quad (7)$$

where $T_{\rm dust}$ is the dust temperature, $x \equiv h\nu/kT_{\rm CMB} \simeq \nu/56.8\,{\rm GHz}$ and ν_0 and $T(\nu_0, \hat{\mathbf{n}})$ are the reference frequency and temperature map, respectively. Now, adopting a dust temperature of 20 K (Abergel et al. 2013a) and assuming that the polarization fraction P/T is the same in the *V*- and *W* bands (for the single thermal dust emission model *only*), the spectral index β for dust emissivity should be approximately 1. However, inspection of Figure 9 of Abergel et al. (2013a) shows that the average spectral index for the Loop I region (see Figure 3) is $\beta_{\rm pl} \simeq 1.6$. (This number is robust as a different $\beta_{\rm pl}$ would lead to a vastly different extrapolated temperature.) Furthermore, our finding $\overline{P_W/P_V} = 1.7$ indicates that the temperature must be closely proportional to frequency, at least in the *V* and *W* bands, i.e., 61–94 GHz.

We thus consider an alternative explanation of the anomalous emission from Loop I, viz. *magnetic* dipole emission from dust grains, arising from thermal fluctuations in the magnetization of grain materials (Draine & Lazarian 1999; Draine & Hensley 2013). It is likely that this emission extends beyond the *W*- and *V* bands. It has been noted that this can be the case if the grain material is ferromagnetic (i.e., enriched with

metallic Fe) or ferrimagnetic (e.g., magnetite, Fe_3O_4). Such grains may generate magnetic dipole emission extending up to 200–300 GHz and it has been argued that this accounts for the surprisingly strong submillimeter and millimeter emission from the Small Magellanic Cloud (Draine & Hensley 2012). This radiation may be particularly strong from the galactic loops too, if a higher fraction of the iron-bearing grains survive after being swept up by the SN blast wave. A population of Fe grains or grains with Fe inclusions at a temperature around 20 K would be expected to produce strong emission due to a ferromagnetic resonance which depends on shape, going up to ∼30 GHz for extreme prolate grains (Draine & Hensley 2013). At 120–130 GHz the magnetic dipole emission from dust grains will drop below the thermal electric dipole "vibrational" emission, while well above 200 GHz its contribution will be negligible relative to thermal emission from dust.

6. CONCLUSION

We have found evidence of local galactic structures such as Loop I in the *WMAP* ILC map of the CMB which is supposedly fully cleaned of foreground emissions. This contamination extends to high galactic latitude so the usual procedure of masking out the Milky Way *cannot* be fully effective at removing it. It extends to sufficiently high frequencies that it cannot be synchrotron radiation but might be magnetic dipole emission from ferro- or ferrimagnetic dust grains, as suggested by theoretical arguments (Draine & Lazarian 1999; Draine & Hensley 2013). This radiation is expected to be *polarized* with a frequency dependent polarization fraction.

It has not escaped our attention that as shown in Figure 1. the lower part of Loop I, in particular the new loop S1 identified by Wolleben (2007), crosses the very region of the sky from which the BICEP 2 experiment has recently detected a *B*-mode polarization signal at 150 GHz (Ade et al. 2014). This has been ascribed to primordial gravitational waves from inflation because "available foreground models" do not correlate with the BICEP maps. The new foreground we have identified is however *not* included in these models. Hence the cosmological significance if any of the detected *B*-mode signal needs further investigation. Forthcoming polarization data from the *Planck* satellite will be crucial in this regard.

We are indebted to Bruce Draine, Pavel Naselsky, and Andrew Strong for helpful discussions and to the Discovery Center for support. We thank the anonymous referee for critical and constructive comments which helped to improve this Letter. We acknowledge use of the `HEALPix`[6] package Górski et al. (2005). Hao Liu is supported by the National Natural Science Foundation of China (grant Nos. 11033003 and 11203024), and the Youth Innovation Promotion Association, CAS. Philipp Mertsch is supported by DoE contract DE-AC02-76SF00515 and a KIPAC Kavli Fellowship. Subir Sarkar acknowledges a DNRF Niels Bohr Professorship.

REFERENCES

Abergel, A., Ade, P. A. R., Aghanim, N., et al. 2013a, arXiv:1312.1300
Abergel, A., Ade, P. A. R., Aghanim, N., et al. 2013b, arXiv:1312.5446
Ade, P., Aghanim, N., Armitage-Caplan, C., et al. 2013a, arXiv:1303.5075
Ade, P., Aghanim, N., Armitage-Caplan, C., et al. 2013b, arXiv:1303.5076
Ade, P., Aghanim, N., Armitage-Caplan, C., et al. 2013c, arXiv:1303.5083
Ade, P., Aghanim, N., Arnaud, M., et al. 2013d, A&A, 554, A139
Ade, P., Aikin, R. W., Barkats, D., et al. 2014, arXiv:1403.3985
Aghanim, N., Arnaud, M., Ashdown, M., et al. 2011, A&A, 536, A26
Aghanim, N., Arnaud, M., Ashdown, M., et al. 2012, A&A, 543, A102
Bennett, C., Larson, D., Weiland, J. L., et al. 2013, ApJS, 208, 20
Berkhuijsen, E. M., Haslam, C. G. T., & Salter, C. J. 1971, A&A, 14, 252
Chiang, L.-Y., Naselsky, P. D., & Coles, P. 2008, MPLA, 23, 1489
Chiang, L.-Y., Naselsky, P. D., Verkhodanov, O. V., & Way, M. J. 2003, ApJL, 590, L65
Copi, C., Huterer, D., Schwarz, D., & Starkman, G. 2007, PhRvD, 75, 023507
Copi, C., Huterer, D., & Starkman, G. 2004, PhRvD, 70, 043515
Cruz, M., Martinez-Gonzalez, E., Vielva, P., et al. 2008, MNRAS, 390, 913
de Oliveira-Costa, A., Tegmark, M., Zaldarriaga, M., & Hamilton, A. 2004, PhRvD, 69, 063516
Draine, B., & Lazarian, A. 1999, ApJ, 512, 740
Draine, B. T., & Hensley, B. 2012, ApJ, 757, 103
Draine, B. T., & Hensley, B. 2013, ApJ, 765, 159
Eriksen, H., Hansen, F., Banday, A., Gorski, K., & Lilje, P. 2004, ApJ, 605, 14
Górski, K. M., Hivon, E., Banday, A. J., et al. 2005, ApJ, 622, 759
Gruppuso, A., Natoli, P., Paci, F., et al. 2013, JCAP, 07, 047
Hansen, F., Banday, A., Gorski, K., Eriksen, H., & Lilje, P. 2009, ApJ, 704, 1448
Hansen, M., Kim, J., Frejsel, A., et al. 2012, JCAP, 10, 059
Hansen, M., Zhao, W., Frejsel, A., et al. 2012, MNRAS, 426, 57
Haslam, C., Salter, C., Stoffel, H., & Wilson, W. 1982, A&AS, 47, 1
Heiles, C., Chu, Y.-H., Troland, T. H., Reynolds, R. J., & Yegingil, I. 1980, ApJ, 242, 533
Hoftuft, J., Eriksen, H., Banday, A., et al. 2009, ApJ, 699, 985
Kim, J., & Naselsky, P. 2010, ApJL, 714, L265
Land, K., & Magueijo, J. 2005, PhRvL, 95, 071301
Land, K., & Magueijo, J. 2007, MNRAS, 378, 153
Larson, D., Dunkley, J., Hinshaw, G., et al. 2011, ApJS, 192, 16
Mertsch, P., & Sarkar, S. 2013, JCAP, 06, 041
Naselsky, P. D., Doroshkevich, A., & Verkhodanov, O. 2004, MNRAS, 349, 695
Naselsky, P. D., & Novikov, D. I. 1995, ApJ, 444, 1
Park, C.-G. 2004, MNRAS, 349, 313
Roger, R. S., Costain, C. H., Landecker, T. L., & Swerdlyk, C. M. 1999, A&AS, 137, 7
Salter, C. J. 1983, BASI, 11, 1
Sarkar, S. 1982, MNRAS, 199, 97
Schwarz, D., Starkman, G., Huterer, D., & Copi, C. 2004, PhRvL, 93, 221301
Wolleben, M. 2007, ApJ, 664, 349

[6] http://healpix.sourceforge.net